The Semiclassical Description of Tunneling in Scattering with Multiple Degrees of Freedom.

G.F. Bonini[a], A.G. Cohen[b], C. Rebbi[b] and V.A. Rubakov[c] *

[a]*Institut für theoretische Physik, University of Heidelberg, D-69120 Heidelberg, Germany*

[b]*Department of Physics, Boston University, Boston, MA 02215, USA*

[c]*Institute for Nuclear Research of the Russian Academy of Sciences, Moscow, 117312, Russian Federation*

Abstract

We describe a computational investigation of tunneling at finite energy in a weakly coupled quantum mechanical system with two degrees of freedom. We compare a full quantum mechanical analysis to the results obtained by making use of a semiclassical technique developed in the context of instanton-like transitions in quantum field theory. This latter technique is based on an analytic continuation of the degrees of freedom into a complex phase space, and the simultaneous analytic continuation of the equations of motion into the complex time plane.

1 Introduction and Motivation

The existence of a small parameter ("coupling constant") in quantum mechanical systems leads to a (typically asymptotic) expansion of observables in powers of this parameter. No other approximation technique has proved

*bonini@thphys.uni-heidelberg.de, cohen@bu.edu, rebbi@bu.edu, rubakov@ms2.inr.ac.ru

as powerful in obtaining physical predictions in such diverse fields as atomic physics, chemistry, quantum field theory, *etc.* Despite these successes, many phenomena in such systems are not amenable to perturbation theory: for example barrier penetration in quantum mechanics does not occur at any order in an (asymptotic) expansion in powers of $\hbar$.

Techniques for dealing with non-perturbative phenomena in theories with a small parameter are far less general. Perhaps the best known example is the WKB approximation, familiar from one-dimensional wave mechanics. A similar technique, the instanton method, is often used to discuss certain non-perturbative phenomena in quantum field theory. But in more complicated cases these methods fail: examples are tunneling at non-zero energy in quantum mechanical systems with more than one degree of freedom, and tunneling processes in quantum field-theoretic models with exclusive initial or final states.

Recently the authors of Ref. [1, 2] have suggested a method for dealing with high-energy processes that proceed through tunneling in weakly coupled quantum field theory. Their technique begins with a path integral representation of the matrix element in question, followed by a double analytic continuation: the fields in the path integral are continued to the complex plane, and in addition the time evolution is continued along a complex contour. In spite of these complications, this technique is essentially semiclassical. The resulting complexified classical system typically remains intractable to analytic methods. Consequently computational techniques must be employed to obtain quantitative results; the feasibility of the corresponding calculations in field theory has been demonstrated in Ref. [3, 4]. We should also stress that the validity of the formalism of Ref. [1, 2] has not been proven, though its plausibility has been supported by comparison with perturbative calculations about the instanton [5, 6].

More specifically, the process under discussion is a non-perturbative instanton mediated transition induced by the collision of two highly energetic particles. Perturbative calculations (see for instance Ref. [7, 8, 9] and references therein) about the instanton suggest that the total cross section has the following functional form

$$\sigma_{2\to\text{any}} \propto e^{-\frac{1}{g^2}F_0(g^2E)} \tag{1}$$

where g is the small coupling constant of the theory and E is the center-of-mass energy. To compute the leading exponent the authors of Ref. [1, 2]

suggested considering an inclusive process with a large number n of incoming particles. They argued that the total probability has a similar form

$$\sigma_{n\to\text{any}} \propto e^{-\frac{1}{g^2}F(g^2E,g^2n)} \tag{2}$$

and that the exponent $F(g^2E, g^2n)$ can be calculated semiclassically by considering a complexified classical system. Furthermore, they conjectured that the two-particle exponent F_0 in Eq. (1) is an appropriate limit of the multiparticle one:

$$F_0(g^2E) = \lim_{g^2n\to 0} F(g^2E, g^2n) \tag{3}$$

Equations (1), (3) on the one hand, and equation (2) on the other, have different status. While the validity of Eq. (2) has been demonstrated by path integral methods (cfr. Section 4), neither the general functional form (1) nor the limiting procedure (3) have been proven so far.

Since the formalism of Ref. [1, 2] has not been rigorously derived from first principles, and the direct evaluation of the resulting path integral, by computer simulation or other numerical procedures is beyond current reach, we have chosen to test the technique by reducing the number of degrees of freedom. In quantum field theoretic models, a general field configuration may be expanded in a complete (infinite) basis of normal modes. In the asymptotic time domains $t \to \pm\infty$ these modes are non-interacting, and the evolution is characterized by a definite particle number. In a semiclassical description of the tunneling process the field evolves through a non-linear regime, and the crucial question is how the particle numbers in the incoming and outgoing asympotic states are related by the non-linear evolution. A minimal model capable of mimicking this dynamics will have some internal degree of freedom, whose excitations at asymptotic times will correspond to the particle number of the field theoretical system, and a non-linear interaction with a barrier, that can be penetrated by tunneling. This can be realized with a system of two particles moving in one dimension. Let the coordinates of these particles be x_1 and x_2, and the dynamics be described by the Lagrangian:

$$L = \frac{1}{4}\dot{x}_1^2 + \frac{1}{4}\dot{x}_2^2 - \frac{1}{8}\omega^2(x_1 - x_2)^2 - V(x_1) \tag{4}$$

where V is an arbitrary positive semi-definite potential which vanishes asymptotically[1]. Since the theory is to be weakly coupled, we assume a potential

[1]We could of course allow V to depend on x_2 as well, provided it does not depend only on the combination $x_1 - x_2$.

of the form

$$V(x) = \frac{1}{g^2} U(g\,x) \tag{5}$$

with $g \ll 1$. For simplicity we will use a gaussian for the potential

$$U(x) \equiv e^{-\frac{1}{2}x^2} \tag{6}$$

although the treatment of other potentials is similar. The properties of the system described by the above Lagrangian are made clearer by replacing the variables x_1, x_2 with the center of mass coordinate $X \equiv (x_1 + x_2)/2$ and the relative coordinate $y \equiv (x_1 - x_2)/2$. With this substitution the Lagrangian takes the form

$$L = \frac{1}{2}\dot{X}^2 + \frac{1}{2}\dot{y}^2 - \frac{1}{2}\omega^2 y^2 - \frac{1}{g^2} e^{-\frac{1}{2}g^2(X+y)^2} \tag{7}$$

and we see that asymptotically it describes the free motion of the center of mass and a decoupled harmonic oscillator. Within the range of the potential, though, the two degrees of freedom are coupled, giving rise to a transfer of energy between them.

In the classical case, the coupling g is an irrelevant parameter: we may rescale the degrees of freedom so that g appears as a universal multiplicative factor. Defining new coordinates $\tilde{X} \equiv gX$, $\tilde{y} \equiv gy$ the Lagrangian becomes

$$L = \frac{1}{g^2}\left[\frac{1}{2}\dot{\tilde{X}}^2 + \frac{1}{2}\dot{\tilde{y}}^2 - \frac{1}{2}\omega^2\tilde{y}^2 - e^{-\frac{1}{2}(\tilde{X}+\tilde{y})^2}\right] \tag{8}$$

The value of g is crucial, however, for the quantum system: the path integral formulation of quantum mechanics together with Eq. (8) show that g^2 plays a role similar to $\hbar$ in determining the magnitude of the quantum fluctuations; the classical limit corresponds to $g^2 \to 0$. This is in close analogy with the field theoretical systems mentioned above. In the following we will use units with $\hbar = 1$ and will characterize the semiclassical treatment as an expansion for small g.

The repulsive potential implies a barrier that must be either overcome or penetrated through tunneling for a transition from an initial state where the center of mass coordinate is approaching the barrier from, *e.g.*, large negative X, to a final state where it is moving away from it towards large positive X. The corresponding transmission probability $\mathcal{T}$ will depend on three quantities: the total initial energy E; the initial energy of the oscillator

E_{osc} (or, equivalently, on its initial quantum number n related to its energy by $E_{osc} = (n + 1/2)\omega$); and the value of g. In analogy with Eq. (1), the transmission probability for an oscillator initially in its ground state as $g \to 0$ has the asymptotic form

$$\mathcal{T}_0(E) = C_0(g^2E)e^{-\frac{1}{g^2}F_0(g^2E)} \tag{9}$$

for some prefactor C_0. Likewise, for a transition from an initial state in the n-th excited level one expects, for $g \to 0$, ng^2 fixed,

$$\mathcal{T}_n(E) = C(g^2E, g^2n)e^{-\frac{1}{g^2}F(g^2E,g^2n)} \tag{10}$$

in analogy to Eq. (2). The advantage of the model we are considering is that the process in question admits a full quantum mechanical treatment as well as the semiclassical analysis. We will present the results of a numerical solution of the full Schrödinger equation and show that the transition from the oscillator ground state can indeed be fitted very well with the expression of Eq. (9). Independently of the semiclassical analysis, this result represents a direct verification of the functional form of Eq. (1), (9). This will be our first conclusion.

We will then use the technique of Ref. [1, 2] and evaluate the function $F(g^2E, g^2n)$ entering Eq. (10) by solving numerically the complexified classical equations on the appropriate contour in the complex time plane. We will thus be able to check the validity of Eq. (3), with the l.h.s., $F_0(g^2E)$, obtained through the full quantum mechanical treatment and the r.h.s., $F(g^2E, g^2n)$, calculated in a semiclassical way. We will show that Eq. (3) indeed holds, and so, in the context of our model at least, we will be able to confirm the conjecture of Ref. [1, 2] by a direct numerical computation. This will be the second main conclusion of this paper.

2 The Classical System

Let us first consider a classical evolution whereby the two particles are initially located on the negative x-axis well outside the range of the potential and their center of mass is moving with positive velocity (*i.e.* toward the barrier). The motion of the system is specified completely by four initial value data. Time translation invariance of the system allows us to choose one of these to be the initial time. It is convenient to take the remaining three

to be the rescaled total energy of the system, $\epsilon \equiv g^2 E$, the rescaled initial oscillator excitation number, $\nu \equiv g^2 n$, (in the classical theory n is *defined* as E_{osc}/ω and need not be integral) and an initial oscillator phase, ϕ. The question at this stage is whether the system can cross to the other side of the barrier, *i.e.* whether the transition is classically allowed. In particular, in the projection to the ν-ϵ plane there will be a classically allowed region where, for some value(s) of ϕ, the system will evolve to the other side of the potential barrier. The rest of the plane will consitute the classically forbidden region where, no matter what the initial phase, the system will bounce back from the barrier.

Clearly the entire domain $\epsilon < 1$ belongs to the classically forbidden region: there can be no classical transition with a total energy smaller than the barrier height (equal to 1 in rescaled units). However, a total energy larger than the barrier height is *per se* no guarantee that the system will cross to the other side of the barrier. The coupling between the center of mass and oscillator degrees of freedom due to the potential will cause a transfer of energy between the two, whose net effect can be repulsion from the barrier even when the total energy is larger than the barrier height. In general, for every initial value of ν there will be some minimal rescaled energy $\epsilon_0(\nu)$ such that for $\epsilon > \epsilon_0$ transitions across the barrier are possible. The function $\epsilon_0(\nu)$ describes the boundary of the classically allowed region.

The minimum of $\epsilon_0(\nu)$ is equal to 1 (*i.e.* to the barrier height). Indeed, there is an obvious, unstable, static solution of the equations of motion with both particles on top of the potential barrier ($x_1(t) = x_2(t) = 0$). This solution, incidentally, corresponds to the static solution called the "sphaleron" in instanton mediated processes [10]. If one perturbs this solution by giving an arbitrarily small, common positive velocity to both particles, they will move in the positive direction toward $X = \infty$. (It is easy to prove that the particles cannot go back over the barrier in this situation. If this were to happen, at some moment in time x_1 would pass through zero. At that moment, by conservation of energy, the magnitude of the center-of-mass velocity could not be larger than the initial velocity of the particles. But a perturbative analysis of the initial motion shows that, however small its initial velocity may be, the center of mass will acquire some finite positive momentum, which will continue to increase so long as $x_1 > 0$. This implies that the magnitude of the center of mass velocity cannot revert to its original arbitrarily small value.) Similarly, the time reversed evolution has the two particles proceeding towards $X = -\infty$. The two evolutions, combined, describe therefore a

classical process where the system goes over the barrier with an energy larger, but arbitrarily close to the barrier height. This evolution, obtained by an infinitesimal perturbation of the "sphaleron", will produce a definite asymptotic value ν_0 of the rescaled initial excitation number, which will characterize the minimum of $\epsilon_0(\nu)$.

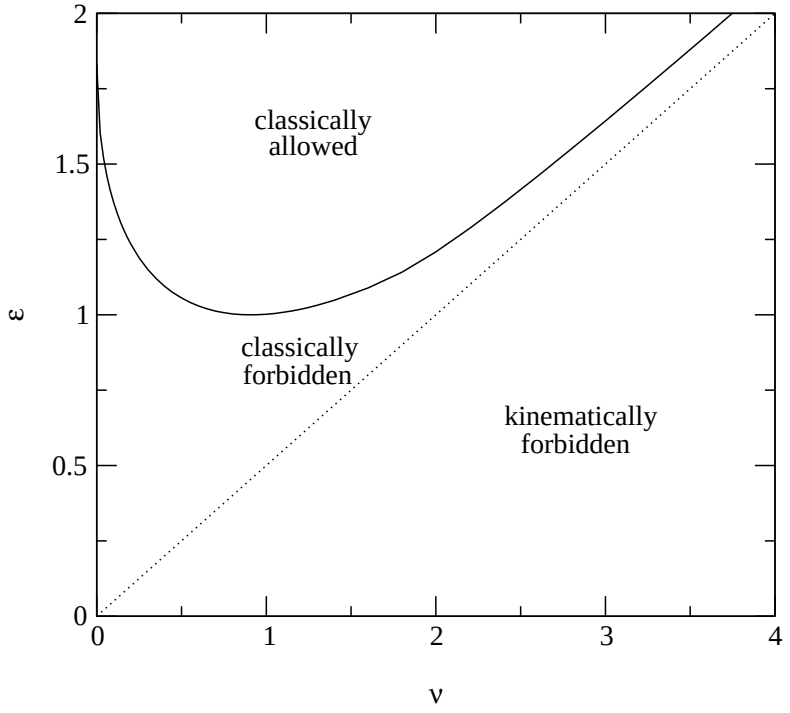

Figure 1: Boundary of the region of classically allowed transitions.

Values of ν smaller or larger than ν_0 will give rise to values $\epsilon_0(\nu)$ larger than the barrier height. Of particular interest for us is $\epsilon_0(0)$, i.e. the lowest energy for which one can have a classically allowed transition with the incoming system in its ground state. In the limiting cases of infinite oscillator strength ($\omega \to \infty$) or of decoupled particles ($\omega = 0$) $\epsilon_0(0)$ takes values 1 and 2, respectively. Indeed, the former case is equivalent to having a single particle (with twice the mass), which will evolve over the barrier as soon as its initial energy is larger than the barrier height. In the second case, the particles proceed independently, sharing the initial energy, and the center of mass will move to positive infinity whenever the particle that feels the

potential will be able to move over the barrier, which of course will happen when its share of the total energy is larger than 1. For finite, non-vanishing values of ω, the value of $\epsilon_0(0)$, or, more generally, $\epsilon_0(\nu)$, must be determined numerically. The small number of degrees of freedom in our model allows us to explore the phase space systematically, varying ϕ, ϵ and ν. In this way we can determine the boundary of the classically allowed region with reasonable accuracy. Throughout this paper we will take $\omega = 1/2$. The corresponding boundary of the classically allowed region is illustrated in Fig. 1. (The dotted line in the figure represents the kinematic boundary $\omega\nu \leq \epsilon$.) With $\omega = 1/2$, $\epsilon_0(0)$ equals approximately 1.8. For energies lower than this value, an incoming system in its ground state may transit the barrier only through tunneling. In the next section we will present a full quantum-mechanical calculation of the corresponding transmission probability $\mathcal{T}_0(E, g)$. In Sect. 4 we will adapt the semiclassical formalism of Ref. [1, 2] to derive an exponential expression for the leading factor in $\mathcal{T}_0$, and calculate the exponent.

It is worthwile to mention that the existence of a definite $\epsilon_0(0)$ where the boundary of classically allowed region meets the axis $\nu = 0$ is one important property which our simplified model, most likely, does not share with its more complex field theoretical counterparts. The infinite number of degrees of freedom of the field theoretic systems opens the possibility that the lower boundary of the classically allowed region approaches the $\nu = 0$ axis only asymptotically, or even that it is bounded below by some non-vanishing minimum ν (cfr. Ref. [11] for a numerical study of classically allowed transitions in the $SU(2)$-Higgs system).

3 Quantum-Mechanical Solution

For the study of the full quantum system it is convenient to use the basis formed by the tensor product of the center-of-mass coordinate basis and the oscillator excitation number basis: $|X\rangle \otimes |n\rangle$. In this basis the state of the system is represented by the multi-component wavefunction

$$\psi_n(X) \equiv (\langle X| \otimes \langle n|)|\Psi\rangle \tag{11}$$

and the time independent Schrödinger equation reads

$$-\frac{\partial^2 \psi_n(X)}{\partial X^2} + \Big(n + \frac{1}{2}\Big)\omega\psi_n(X) + \sum_{n'} V_{n,n'}(X)\psi_{n'}(X) = E\psi_n(X) \tag{12}$$

where

$$V_{n,n'}(X) = \langle n|\frac{1}{g^2}e^{-\frac{1}{2}g^2(X+y)}|n'\rangle \tag{13}$$

In the asymptotic region (large $|X|$) the interaction terms are negligible, and the solution takes the form

$$\lim_{X\to\pm\infty}\psi_n(X) = t_n^{\pm}e^{\imath k_n X} + r_n^{\pm}e^{-\imath k_n X} \tag{14}$$

with

$$k_n = \sqrt{E-(n+\frac{1}{2})\omega} \tag{15}$$

When $n > E - \omega/2$, k_n becomes imaginary; we fix the continuation by defining

$$k_n = \imath\sqrt{(n+\frac{1}{2})\omega - E} \tag{16}$$

In order to calculate the transmission probability, we will look for a solution with

$$t_n^- = \delta_{n,0} \tag{17}$$

and

$$r_n^+ = 0 \tag{18}$$

(This corresponds to an incoming system in its ground state. The generalization to a process with an incoming excited state is straightforward.) The inhomogeneous boundary conditions (17), (18) fix the solution completely and the transmission probability is then given by

$$\mathcal{T}_0 = \sum_{n\le E/\omega-1/2}\frac{k_n}{k_0}|t_n^+|^2 \tag{19}$$

Numerical methods may be used to calculate the solution satisfying the boundary conditions (18), (17), and therefore also $\mathcal{T}_0$. In the rest of this section we outline our computational procedure and describe the result.

To solve the Schrödinger equation numerically we must discretize and truncate the system to leave a finite, albeit very large, number of unknowns. We accomplish this by replacing the continuum X-axis with a discrete and finite set of equally spaced vertices

$$X_i = ia \tag{20}$$

where a denotes the lattice spacing and $-N_x \leq i \leq N_x$. The truncation in oscillator space is perfomed by restricting $n \leq N_o$.

To keep our notation concise, we will omit the oscillator indices, using implicit vector and matrix notation, and will use subscripts for the locations along the X axis. Thus, for instance, the expression $\sum_{n'} V_{n,n'}(ia)\psi_{n'}(ia)$ will be simply written as $V_i\psi_i$. It is also convenient to rewrite the continuum equation in the form

$$\frac{\partial^2\psi(X)}{\partial X^2} = A(X)\psi(X) \tag{21}$$

where the matrix $A(X)$ is given by

$$A_{n,n'}(X) = \Big[(n+\frac{1}{2})\omega - E\Big]\delta_{n,n'} + V_{n,n'}(X) \tag{22}$$

The discretization of Eq. (21) could be accomplished in a straightforward manner by using the central difference approximation of the second derivative with respect to X

$$\partial^2\psi(X)/\partial X^2 = \frac{\psi(X+a)+\psi(X-a)-2\psi(X)}{a^2} + O(a^2) \tag{23}$$

This would give the equations

$$\psi_{i+1} - 2\psi_i + \psi_{i-1} = A_i\psi_i \tag{24}$$

with an error $O(a^4)$.

We have actually used the more sophisticated Numerov-Cowling algorithm, which allows us to improve the accuracy of the discretization by two powers of a. From the Taylor series expansion of $\psi(X)$ we immediately find

$$\psi_{i+1} + \psi_{i-1} - 2\psi_i = \left[\frac{\partial^2\psi}{\partial X^2}\right]_i a^2 + \left[\frac{\partial^4\psi}{\partial X^4}\right]_i \frac{a^4}{12} + O(a^6) \tag{25}$$

Using Eq. (21), $(\partial^4\psi/\partial X^4)(a^4/12)$ can be written as $(\partial^2 A\psi/\partial X^2)(a^4/12)$; this can be in turn approximated by $(A_{i+1}\psi_{i+1} + A_{i-1}\psi_{i-1} - 2A_i\psi_i)(a^2/12)$ with the same level of accuracy. We are thus finally led to the following discretization of eq.(21):

$$\psi_{i+1} - 2\psi_i + \psi_{i-1} = \frac{a^2}{12}A_{i+1}\psi_{i+1} + \frac{5a^2}{6}A_i\psi_i + \frac{a^2}{12}A_{i-1}\psi_{i-1} \tag{26}$$

which entails an error of order a^6.

Before proceeding further, we turn for a moment to the calculation of the matrix elements $V_{n,n'}(X)$, which are needed for solving the Schrödinger equation. These can be calculated very efficiently by means of a recursion procedure. $V_{n,n'}(X)$ is given by

$$V_{n,n'}(X) = \frac{1}{g^2} \langle v_n | v_{n'} \rangle \tag{27}$$

where $|v_n\rangle$ denotes the state

$$|v_n\rangle = e^{-\frac{1}{4}g^2(X+y)^2} |n\rangle \tag{28}$$

It is convenient to use the y coordinate representation, writing

$$|v_n\rangle = e^{-\frac{1}{4}g^2(X+y)^2} \frac{(a^\dagger)^n}{\sqrt{n!}} \Big(\frac{\omega}{\pi}\Big)^{1/4} e^{-\frac{1}{2}\omega y^2} \tag{29}$$

with

$$\begin{aligned} a &= \frac{1}{\sqrt{2\omega}} \frac{d}{dy} + \sqrt{\frac{\omega}{2}} y \\ a^\dagger &= -\frac{1}{\sqrt{2\omega}} \frac{d}{dy} + \sqrt{\frac{\omega}{2}} y \end{aligned} \tag{30}$$

The first exponential in Eq. (29) can be brought to the right, using

$$e^{-\frac{1}{4}g^2(X+y)^2} a^\dagger = \Big(a^\dagger - \frac{g^2}{2\sqrt{2\omega}}(X+y)\Big) e^{-\frac{1}{4}g^2(X+y)^2} \tag{31}$$

This gives

$$|v_n\rangle = \frac{1}{\sqrt{n!}} \Big(\frac{\omega}{\pi}\Big)^{1/4} \Big(a^\dagger - \frac{g^2}{2\sqrt{2\omega}}(X+y)\Big)^n e^{-\frac{1}{4}g^2(X+y)^2 - \frac{1}{2}\omega y^2} \tag{32}$$

The exponential on the r.h.s. may be written as a constant times the ground state wavefunction of a shifted oscillator with frequency Ω:

$$e^{-\frac{1}{4}g^2(X+y)^2 - \frac{1}{2}\omega y^2} = \Big(\frac{\pi}{\Omega}\Big)^{1/4} e^{-\frac{g^2\omega}{4\Omega}X^2} \Big(\frac{\Omega}{\pi}\Big)^{1/4} e^{-\frac{1}{2}\Omega z^2} \tag{33}$$

with

$$\Omega = \omega + \frac{g^2}{2} \tag{34}$$

$$z = y + \frac{g^2}{2\Omega} X \tag{35}$$

Re-expressing everything in terms of the creation and annihilation operators for this new oscillator

$$\begin{aligned} b &= \frac{1}{\sqrt{2\Omega}} \frac{d}{dz} + \sqrt{\frac{\Omega}{2}} z \\ b^\dagger &= -\frac{1}{\sqrt{2\Omega}} \frac{d}{dz} + \sqrt{\frac{\Omega}{2}} z \end{aligned} \tag{36}$$

we find

$$|v_n\rangle = \frac{1}{\sqrt{n!}} \Big(\frac{\omega}{\Omega}\Big)^{1/4} e^{-\frac{g^2\omega}{4\Omega} X^2} \Big(\alpha b^\dagger + \beta b + \gamma\Big)^n |0\rangle_b \tag{37}$$

with

$$\begin{aligned} \alpha &= \sqrt{\frac{\omega}{\Omega}} \\ \beta &= -\frac{g^2}{2\sqrt{\omega\Omega}} \\ \gamma &= -\frac{g^2}{\Omega} \sqrt{\frac{\omega}{2}}\, X \ . \end{aligned} \tag{38}$$

It is now straightforward to calculate the components of of $|v_n\rangle$ in the b-oscillator basis, and therefore also the inner products $\langle v_n | v_{n'} \rangle$, by numerical iteration.

In order to solve the discretized Schrödinger equation, we must calculate $\psi_{i,n}$ (with the oscillator index explicit) for $-N_x \le i \le N_x$, $0 \le n \le N_o$. This amounts to $2(N_x+1)N_o$ complex variables. These satisfy Eq. (26), for $N_x + 1 \le i \le N_x - 1$, for a total of $2(N_x-1)N_o$ complex conditions. In addition, the boundary Eq. (17), (18) give us the $2N_o$ complex conditions[2]

$$\begin{aligned} \psi_{-N_x,0} &= e^{\imath k_0 a} \psi_{-N_x+1,0} + (1 - e^{\imath k_0 a}) \\ \psi_{-N_x,n} &= e^{\imath k_n a} \psi_{-N_x+1,n} \qquad n > 0 \\ \psi_{N_x,n} &= e^{\imath k_n a} \psi_{N_x-1,n} \end{aligned} \tag{39}$$

[2]In these equations we can use either the k_n given by the continuum dispersion formula Eq. (15) or those given by the dispersion formula that follows from Eq. (21). Given the high accuracy of the Numerov-Cowling discretization, the two options produce practically indistinguishable results.

Altogether, we thus have a system of $2(N_x+1)N_o$ complex, non-homogeneous linear equations, which is precisely the number needed to determine all of the unknowns. In order to insure good accuracy of the solution, we found it prudent to use cut-off values as large as $N_x = 4096$ and $N_o = 400$. With such numbers it would be impossible to tackle the system by brute force using a general purpose solver: this corresponds to a system of over 3 million complex equations, which could not possibly be solved by a general purpose procedure. However, we can take advantage of the special form of Eq. (26) to implement an efficient solution procedure. Indeed, by inverting a set of $(N_o+1)\times(N_o+1)$ matrices, which is computationally feasible, Eq. (21) can be recast in the form

$$\psi_i = L_i\psi_{i-1} + R_i\psi_{i+1} \tag{40}$$

where L_i and R_i are again $(N_o+1)\times(N_o+1)$ matrices. The elimination of any definite ψ_i now leads to a system of equations for the remaining variables which, with $(N_o+1)\times(N_o+1)$ matrix algebra and matrix inversion, can be brought to the same form of Eq. (40), with suitably redefined L and R matrices. We have used this procedure to progressively eliminate all the intermediate variables ψ_i, $i = -N_x+1 \ldots N_x-1$, ultimately leaving a system of equations linearly relating all ψ_i to ψ_{-N_x} and ψ_{N_x}. (Loosely speaking, the procedure can be considered the implementation of a Green's function for our discretized system of equations.) In particular, ψ_{-N_x+1} and ψ_{N_x-1} are thus given as linear combinations of ψ_{-N_x} and ψ_{N_x}. Substituting these linear combinations in Eq. (39) we now obtain a system of $2N_o+2$ complex, linear, non-homogeneous equations for the $2N_o+2$ complex variables ψ_{-N_x}, ψ_{N_x}, which can be easily solved numerically. As a final remark, we observe that the solution procedure outlined above only requires manipulation of real matrices for the elimination of the intermediate variables, which entails a substantial saving of memory and processor time. Moreover, we can also take advantage of the obvious symmetry under reflection of the X-axis to further halve the computational costs.

For our numerical calculations we have used $\omega = 0.5$ for the oscillator constant. We have found this value a good middle ground betweeen the extremes of very tight and very loose oscillator coupling, where the novel features introduced by the internal degree of freedom become less evident. Also, apart from some calculations where we varied parameters to study the effects of the discretization, we have used a cut-off $N_x = 2048$ and a lattice spacing $a = 0.03\sqrt{2}$. Insofar as N_o is concerned, we insured that its

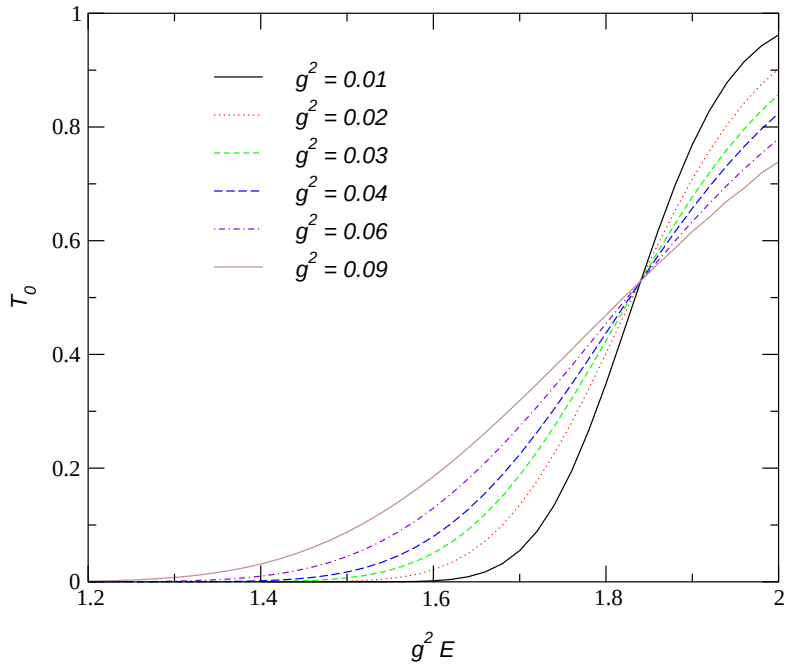

Figure 2: Transmission probability as function of rescaled total energy.

g^2E	$g^2=0.01$	$g^2=0.02$	$g^2=0.03$	$g^2=0.04$	$g^2=0.06$	$g^2=0.09$	$-F$
1.00						0.00000241	-1.1520
1.04					0.00000004	0.00001080	-0.9906
1.08					0.00000039	0.00004266	-0.8446
1.12				0.00000001	0.00000269	0.00014584	-0.7143
1.16				0.00000010	0.00001472	0.00043282	-0.5477
1.20			0.00000001	0.00000094	0.00006497	0.00112833	-0.5051
1.24			0.00000020	0.00000689	0.00023717	0.00262162	-0.4254
1.28			0.00000203	0.00003837	0.00073434	0.00550586	-0.3603
1.32		0.00000011	0.00001539	0.00017019	0.00197114	0.01058551	-0.2948
1.36		0.00000165	0.00008629	0.00062109	0.00467386	0.01883914	-0.2375
1.40		0.00001644	0.00038313	0.00191059	0.00994856	0.03133460	-0.1889
1.44	0.00000003	0.00011153	0.00139099	0.00506866	0.01926910	0.04910559	-0.1625
1.48	0.00000130	0.00057657	0.00423391	0.01182169	0.03435230	0.07301430	-0.1220
1.52	0.00002648	0.00234899	0.01103532	0.02460109	0.05692140	0.10362365	-0.0897
1.56	0.00026569	0.00775891	0.02508580	0.04629424	0.08840244	0.14111159	-0.0675
1.60	0.00181804	0.02128779	0.05054193	0.07972148	0.12963479	0.18520851	-0.0492
1.64	0.00886218	0.04956287	0.09149895	0.12687764	0.18064354	0.23519177	-0.0344
1.68	0.03199884	0.09978377	0.15067840	0.18832587	0.24056017	0.28995637	-0.0227
1.72	0.08854723	0.17673890	0.22824543	0.26278176	0.30770372	0.34813584	-0.0138
1.76	0.19415580	0.27975333	0.32121430	0.34722470	0.37974509	0.40829435	-0.0073
1.80	0.34839619	0.40164508	0.42390234	0.43740276	0.45411756	0.46898820	-0.0028
1.84	0.52777191	0.53035499	0.52913755	0.52842410	0.52816695	0.52887867	-0.0001

Table 1: Results for the transmission probability.

value is large enough that the cut-off energy $(N_o+1/2)\omega$ exceeds the barrier height by at least a factor of two. We have also checked that the highest modes are essentially uncoupled. Specifically, we have used $N_o = 400$ for $g^2 = 0.01$ and $g^2 = 0.02$ and $N_o = 200$ for all other values of g^2 (namely $g^2 = 0.03,\ 0.04,\ 0.06$ and 0.09). We have solved the Schrödinger equation for values of g^2E ranging between 1 and 2 in steps of 0.02. A slightly thinned out compilation of our data is presented in Table 1.

Our results are also illustrated in Fig. 2. The approach to the classical limit (a step function at $g^2E = \epsilon_0(0)$) is evident. In Fig. 3 we plot the logarithm of the transmission probability as function of $1/g^2$ for 8 values of g^2E equally spaced between 1.1 and 1.8. The conjecture following from the semiclassical treatment is that for small g^2 the logarithm of the transmission probability should exhibit the linear behavior in $1/g^2$ at fixed g^2E

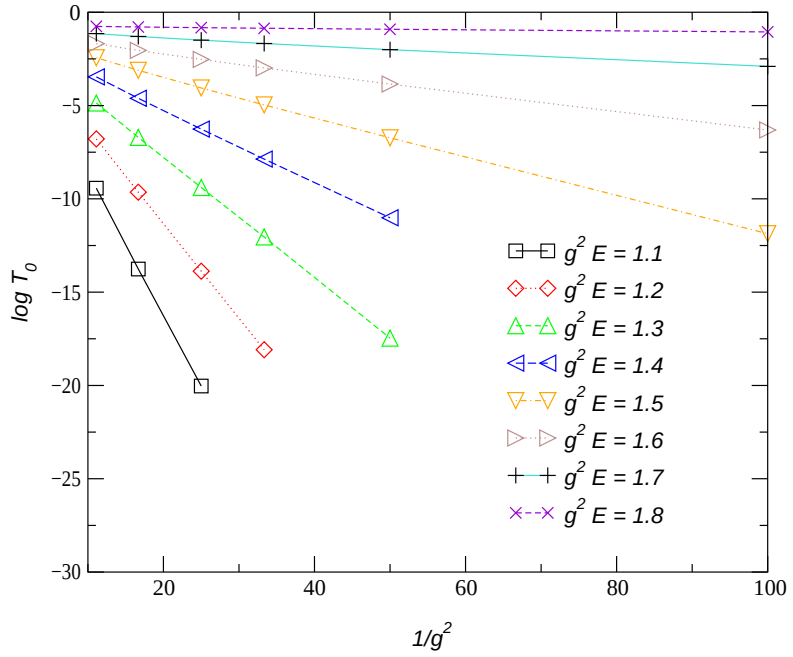

Figure 3: Logarithm of the transmission probability as function of $1/g^2$.

N_o	a	N_x	$\mathcal{T}_0$
200	0.05	1024	0.18435
200	0.03	2048	0.18727
250	0.03	2048	0.18728
200	0.025	2048	0.18750
200	0.025	4096	0.18750
250	0.025	2048	0.18750
250	0.02	2048	0.18759

Table 2: Check of discretization effects.

(cfr. Eq. (9))

$$\log \mathcal{T}_0 = \log C_0(g^2 E) - \frac{1}{g^2} F_0(g^2 E) \tag{41}$$

This is well supported by the data in Fig. 3. We have used the slope of the last segment (*i.e.* the segment corresponding to the two largest $1/g^2$) for which we have significant data to derive the values of F_0 reproduced in Table 1. In the next section we will compare them to the results of a semiclassical calculation.

Finally, we performed several checks to estimate the accuracy of our numerical calculations. For all solutions we verified the degree to which the unitarity constraint

$$\sum_{n \leq E/\omega - 1/2} \frac{k_n}{k_0} (|t_n^+|^2 + |r_n^-|^2) = 1 \tag{42}$$

was satisfied. We found this equation fulfilled with an error ranging from 10^{-6} to 10^{-5}. One might object that some of the data for $\mathcal{T}_0$ in Table 1 are much smaller than this error. This does not necessarily invalidate them, as our use of a discretized Green function may capture the correct exponential decays with relative, rather than absolute errors, of the above order of magnitude. The regularity in even the smallest entries in the Table 1 supports this argument. In any event, even discarding all values of $\mathcal{T}_0 \leq 10^{-5}$ one would still be left with a rich sample of data verifying Eq. (41).

We have checked the effects of the cut-offs and of the finiteness of the lattice spacing by repeating the calculation (for $g^2 = 0.03,\ g^2 E = 1.7$) with different values of N_x, N_o and a. The results are reproduced in Table 2 which indicates that, apart from the case of a substantial increase in a, the relative errors due to the discretization are of order 10^{-3}.

An alternative approach to the calculation of $\mathcal{T}_0$ consists in solving the time-dependent Schrödinger equation. One can simulate then the collision of a wave packet against the barrier and measure directly the trasmission probability. It is of course crucial to implement a solution scheme which preserves the unitarity of the evolution (up to numerical round-off errors). We did follow this approach in some earlier calculations, using a split operator technique to achieve a unitary evolution. We obtained results consistent with our later calculations based on the time independent Schrödinger equation. However solving the time dependent Schrödinger equation proved much more (CP) time consuming than solving the time independent one and so we abandoned the former method in favor of the technique described in this section.

4 The Semi-Classical Formalism

We begin this Section with the derivation of the semi-classical procedure for calculating the exponent $F(g^2E, g^2n)$ of the transmission probability from the n-th excited state at total energy E, Eq.(10). Consider an incoming state of the form

$$|E,n\rangle_\delta = \int dP' \Phi_{P,\delta}(P')|P',n> \tag{43}$$

where

$$P = \sqrt{2(E-\omega n)}\ , \tag{44}$$

$$|P',n>= \frac{1}{\sqrt{2\pi}} \int dX e^{\imath P' X}|X\rangle \otimes |n\rangle \tag{45}$$

is a simultaneous eigenstate of the center of mass momentum and oscillator number, and $\Phi_{P,\delta}(P')$ is a momentum space wavefunction with the following properties:

- it is sharply peaked for $P' \approx P$, with a width of order δ;
- it corresponds to an X-space wave packet which has support only for $X \ll 0$, well outside of the range of the potential.

With these definitions, the transmission probability is given by

$$\mathcal{T}_n(E) = \lim_{\delta\to 0} \lim_{t_f - t_i \to \infty} \int_0^\infty dX_f \int_{-\infty}^\infty dy_f \, |\langle X_f, y_f|e^{-\imath H(t_f-t_i)}|E,n\rangle_\delta|^2 \tag{46}$$

This motivates us to calculate the matrix element

$$A(X_f, y_f, P, n) = \langle X_f, y_f | e^{-\imath H(t_f - t_i)} | P, n \rangle \tag{47}$$

Position-eigenstate matrix elements may be evaluated in terms of a path integral involving the classical action:

$$\langle X_f, y_f | e^{-\imath H(t_f - t_i)} | X_i, y_i \rangle = C \int [dX][dy]\, e^{\imath S} \tag{48}$$

where C is a normalization constant, and the integration is over paths satisfying $X(t_i) = X_i,\ y(t_i) = y_i$ and $X(t_f) = X_f,\ y(t_f) = y_f$. The amplitude (47) is the convolution of the path integral (48) with the eigenfunctions of the center-of-mass momentum and oscillator excitation number, $e^{\imath PX}$ and $\langle y|n\rangle$, respectively. $\langle y|n\rangle$ is conveniently represented in terms of an integral over coherent state variables z and $\bar{z}$. In this way we obtain

$$\begin{aligned} A(X_f, y_f, P, n) = \frac{1}{\sqrt{2\pi}} \int dX_i\, dy_i\, e^{\imath P X_i} \int \frac{dz d\bar{z}}{2\pi\imath}\, e^{-\bar{z}z} \frac{\bar{z}^n}{\sqrt{n!}} \\ e^{-\frac{1}{2}z^2 - \frac{1}{2}\omega y_i^2 + \sqrt{2\omega} z y_i} \langle X_f, y_f | e^{-\imath H(t_f - t_i)} | X_i, y_i \rangle \end{aligned} \tag{49}$$

The main idea, adapted from the method of Ref. [1, 2], is to set $E = \epsilon/g^2$, $n = \nu/g^2$ and take the limit $g \to 0$ while holding ϵ, ν fixed. Indeed, by rescaling the integration variables, we are then able to recast the matrix element in the form:

$$A = C \int dX_i\, dy_i \int \frac{dz d\bar{z}}{2\pi i} \int [dX][dy]\, e^{-\frac{1}{g^2}\Gamma} \tag{50}$$

with

$$\Gamma = -\imath S + \frac{1}{2}z^2 + \frac{1}{2}\omega y_i^2 - \sqrt{2\omega} z y_i + \bar{z}z - \imath p X_i - \nu \ln \bar{z} + \frac{1}{2}\nu(\ln \nu - 1) \tag{51}$$

where $p = gP$, S is the classical action, and Stirling's approximation has been used for the factorial[3].

This form for the matrix element A is now suitable for a semiclassical analysis at small g: we find stationary points of Γ, and evaluate the integral

[3]In order to keep our notation simple, we have used the same symbols (*i.e.* X_i, y_i) for all rescaled integration variables. Note that X_f and y_f must also be eventually integrated upon, cfr. Eq. (46), and are rescaled as well.

in a gaussian approximation about such points. The stationarity conditions (obtained by varying $X(t), y(t), X_i, \bar{z}, z$, and y_i) are:

$$\frac{\delta S}{\delta X(t)} = \frac{\delta S}{\delta y(t)} = 0 \ , \quad t \neq t_i, t_f \tag{52}$$

$$\left.\frac{dX}{dt}\right|_{t=t_i} = p \tag{53}$$

$$\begin{aligned} \bar{z}z &= \nu \\ \left(\omega y_i + \imath \left.\frac{dy}{dt}\right|_{t=t_i}\right) &= \sqrt{2\omega}\, z \\ \left(\omega y_i - \imath \left.\frac{dy}{dt}\right|_{t=t_i}\right) &= \sqrt{2\omega}\, \bar{z} \end{aligned} \tag{54}$$

As expected, Eq. (52) is the classical equation of motion for this system, while Eq. (53) and (54) imply that the initial classical state has the (rescaled) center-of-mass momentum p and oscillator excitation number ν, so that $\epsilon = p^2/2 + \omega\nu$. Therefore in the classically forbidden region of the $\epsilon - \nu$ plane there will be no real solution where the system goes over the barrier. Nevertheless there may be *complex* solutions. We expect that the integral is dominated by stationary points, even if these points lie outside the domain of integration. Hence we will seek solutions that may involve complex values for the integration variables[4]. In searching for such solutions we must remember that we are performing an analytic continuation of the integration variables; in general we will run into singularities in the complex t-plane. To deal with this problem we note that the *time* contour, the real time axis, can be distorted into the complex plane without changing the path integral, provided we keep the time contour end points (t_i, t_f) fixed[5]. Thus our strategy will be to search for complex solutions to Eq. (54) along a complex time contour $ABCDE$ as shown in Fig. 4.

The matrix element (47) in this approximation becomes

$$A = e^{-\frac{1}{g^2}\Gamma(p,n,X_f,y_f)+c} \tag{55}$$

[4]In general this allows values of z and $\bar{z}$ such that $\bar{z} \neq z^*$.

[5]The evolution operator may be written $\exp[-\imath H(t_f - t_i)] = \prod_j \exp[-\imath H dt_j]$ provided $\sum_j dt_j = (t_f - t_i)$. This argument applies even for complex dt_j.

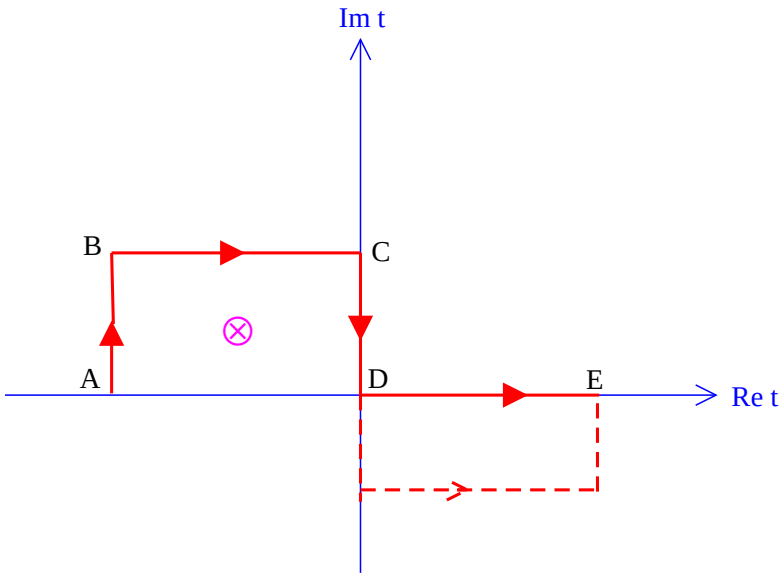

Figure 4: Contours in the complex time plane used to find the saddle point solutions.

where the correction c determines a pre-exponential factor in the semiclassical limit, *i.e.* $\lim_{g\to 0} g^2 c = 0$. The function Γ is equal to the right hand side of Eq. (51) evaluated at the solution to Eq. (52-54). Using these equations to eliminate z we write

$$\Gamma = -\imath S_0 - \imath\frac{1}{2}pX_i - \nu\ln\bar{z} + \frac{1}{2}\nu\ln\nu \tag{56}$$

where

$$S_0 = -\int_{t_i}^{t_f} dt\left[\frac{1}{2}X\frac{d^2}{dt^2}X + \frac{1}{2}y(\frac{d^2}{dt^2}+\omega^2)y + e^{-(X+y)^2}\right] + \frac{1}{2}X_f\frac{dX}{dt}\bigg|_{t=t_f} + \frac{1}{2}y_f\frac{dy}{dt}\bigg|_{t=t_f} \tag{57}$$

Note that the quantity S_0 is insensitive to the value of t_i, provided the solution to Eq. (52) is in the asymptotic region near time t_i.

Equations (53), (54) and (56) involve the quantities defined at large negative time on the real time axis (region A in Fig. 4). It is convenient to formulate the boundary conditions at large negative Re t on the part BC of the contour, where

$$t = t' + \frac{\imath}{2}T\ , \quad t' = \text{real} \to -\infty$$

Since for the moment we consider the asymptotic past, we may ignore the potential V and write the solution at large negative t' as follows,

$$y(t) = \frac{1}{\sqrt{2\omega}}(ue^{-\imath\omega t'} + ve^{\imath\omega t'}) \tag{58}$$

$$X(t) = X_0 + pt' \tag{59}$$

The three parameters of the solution, X_0, u and v, which are in general complex, are related to the quantities entering Eq. (53), (54), (56) in an obvious way,

$$ue^{-\frac{1}{2}\omega T} = ze^{\imath\omega t_i}\ , \quad ve^{\frac{1}{2}\omega T} = \bar{z}e^{-\imath\omega t_i}\ ,$$

$$X_i = X_0 - \frac{\imath}{2}pT + pt_i$$

The condition

$$\bar{z}z \equiv uv = \nu \tag{60}$$

tells us that the phase of u is opposite to that of v, and we may parametrize them as

$$v = e^{\theta}u^* \tag{61}$$

So far we have not specified a value for the parameter T; we have argued that our result is independent of this parameter, provided we avoid singularities in the complex plane. Since variation of T changes the value of Im X_0, we can adjust T such that X is real in the region B: Im $X_0 = 0$.

The transition probability is given by the absolute value of the matrix element squared; that is, in terms of twice the real part of Γ. Using the above relations between u and v we can write the transmission probability as $\exp(-F/g^2)$ where

$$F = 2\text{Im } S_0 - \epsilon T - \nu\theta \tag{62}$$

The resulting values of T and θ depend on ν and ϵ. However, we may treat T and θ as independent parameters instead, so that the boundary conditions are formulated in a simple way in the asymptotic past on the part BC of the contour:

(i) $X(t')$ and $\dot{X}(t')$ are real at B.

(ii) positive and negative frequency parts of the oscillator solution (58) are related by Eq. (61) at B.

At given T and θ, the initial center-of-mass momentum and excitation number (and hence the total energy) are to be found from Eq. (53) and (60). It is straightforward to check that

$$\frac{\partial\,(2\text{Im } S_0(T,\theta))}{\partial T} = \epsilon$$

$$\frac{\partial\,(2\text{Im } S_0(T,\theta))}{\partial \theta} = \nu$$

so that T and θ are Legendre conjugate to ϵ and ν. It is worth noting also that Eq. (61) at $\theta \neq 0$ in fact *requires* the solution to be complex in the region B of the contour.

We are interested in the total probability for transmission; thus we should integrate our probability over all values of y_f and over positive values of X_f. This final integral may also be done using the saddle point approximation. The saddle point condition is simply that

(iii) the solution $X(t)$ and $y(t)$ should be *real* along the $D \to E$ part of the contour.

At given T and θ, the classical equations of motion and the boundary conditions (i), (ii) and (iii) are sufficient to specify the complex solution up to time translations along the real axis. Finding the solutions is still a non-trivial computational task. To simplify this task we start from a sub-class

of solutions with $\theta = 0$, whose numerical determination is easier, and then deform these solutions to $\theta \neq 0$.

For the solutions with $\theta = 0$ the X and y coordinates are analytic and real along the entire contour $BCDE$ of Fig. 4. From the Cauchy-Riemann conditions it follows that the velocities $\dot{X}$ and $\dot{y}$ vanish at C and D. The motion along the imaginary time axis can be reformulated in terms of $\tau =$ Im t and a "Euclidean" Lagrangian

$$L = \left[\frac{1}{2}\frac{dX}{d\tau}^2 + \frac{1}{2}\dot{y}^2 + \frac{1}{2}\omega^2 y^2 + e^{-\frac{1}{2}(X+y)^2}\right] \tag{63}$$

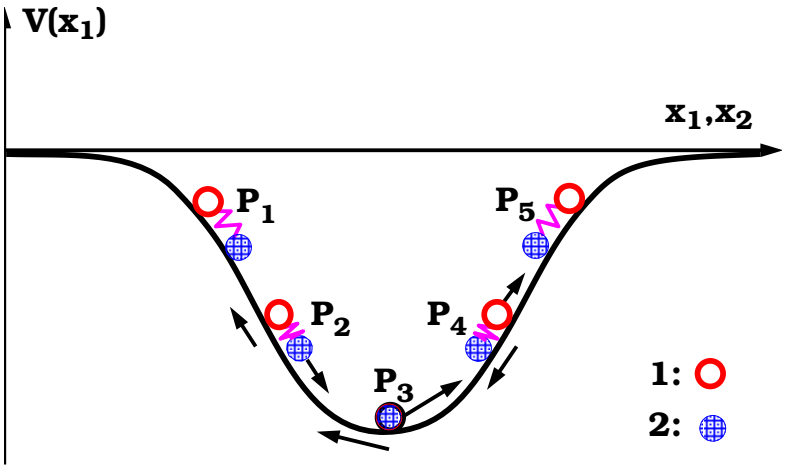

Figure 5: Motion in the "periodic instanton" solutions.

The equations of motion

$$\begin{aligned} \frac{d^2X}{d\tau^2} &= -(X+y)e^{-\frac{1}{2}(X+y)^2} \\ \frac{d^2y}{d\tau^2} &= \omega^2 y - (X+y)e^{-\frac{1}{2}(X+y)^2} \end{aligned} \tag{64}$$

describe the evolution of the system along the imaginary time axis. We look for periodic solutions where $dX/d\tau$ and $dy/d\tau$ vanish at the turning points $\tau = 0$ and $\tau = T/2$, T being the period of the motion. These solutions are analogous to the Euclidean solutions that are commonly used to describe

motion through a barrier in the semiclassical treatment of tunneling with a single degree of freedom. In this latter case finding periodic solutions is straightforward: one need only integrate the equations of motion with inverted potential. The situation with several degrees of freedom is not so simple. Indeed, the continuation to imaginary time not only inverts the potential barrier, which now becomes a potential well, but also changes the harmonic restoring force into a linearly increasing repulsive force. This force makes the system unstable, requiring careful adjustment of the values of X and y at the turning points to obtain a periodic solution. The resulting motion is similar to the "periodic instanton" solutions that appear in topology changing transitions in quantum field theory [12]. There too, all of the field oscillator degrees of freedom become repulsive in the Euclidean motion and the solutions are unstable: a small perturbation of the field profile at one of the turning points grows exponentially in the subsequent evolution. The motion in the "periodic instanton" solutions of our model is illustrated in Fig. 5. At the turning points (P_1, P_5) particle 1 is attracted towards the bottom of the potential well but repelled by particle 2, which is located between particle 1 and the bottom of the potential. Both particles accelerate towards the bottom (particle 2 because of the repulsive force exerted by particle 1). The balance of forces, however, is such that particle 1 moves faster than particle 2, reducing the interparticle distance (P_2, P_4) and, correspondingly, the repulsive force, until it overtakes particle 2 precisely when both particles transit through the bottom of the potential (P_3).

Finding the periodic instanton solutions of our model is rather easy. We divide the interval $0 \leq \tau \leq T/4$ into N subintervals of width $\Delta\tau = T/(4N)$ and we denote by X_i, y_i the values taken by X and y at $\tau = i\Delta\tau$. We discretize the Euclidean action $S_E = \int L_E \, d\tau$ and look for a minimum of S_E with respect to the variables $X_i, y_i, \quad i = 0 \ldots N-1$, while X_N and y_N are kept fixed at zero. Since the Euclidean action is bounded from below, the algorithm of conjugate gradients converges rapidly to the correct solution. The values X_0, y_0 can then be used as initial data for the integration of the equations of motion along the real time axis (from D to E in Fig. 4) until both particles are far out of range of the potential. In this manner one can find the asymptotic oscillator number of the solutions (in the periodic instanton solutions initial and final oscillator numbers are of course identical). The periodic instanton solutions span the one-dimensional subspace denoted by the thick line in the ν-ϵ plot of Fig. 6.

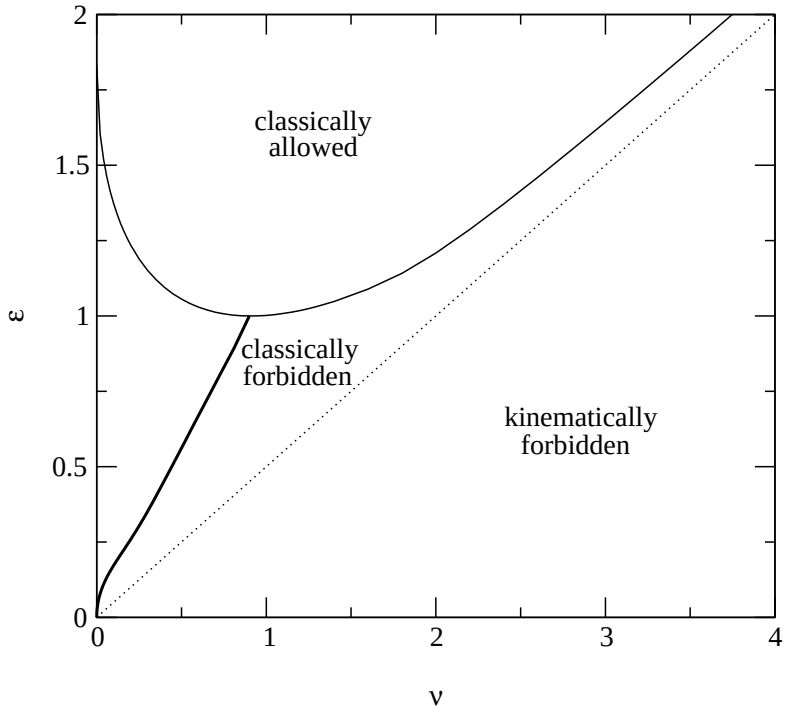

Figure 6: The curve spanned by the periodic instanton solutions.

Starting from the periodic instanton solutions we find solutions with $\theta > 0$ and reduced incoming oscillator number ν by a deformation procedure. In order to solve the equations of motion numerically we subdivide the contour BCD of Fig. 4 into N subintervals separated by vertices labeled by an index $i = 0 \ldots N$. We denote by δt_i the time interval from vertex i to vertex $i+1$. δt_i will be real along the BC portion of the contour, after which δt_i should be negative imaginary. It is convenient, however, to place the very last subinterval along the real time axis. Thus we place the vertex $N-1$ at the origin, and the vertex N at the point $t = \delta t_{N-1} =$ real. The discretized action is

$$\begin{aligned} S &= \sum_{i=0}^{N-1} \Bigg[\frac{(X_{i+1} - X_i)^2}{2\delta t_i} + \frac{(y_{i+1} - y_i)^2}{2\delta t_i} \\ &\quad -\omega^2 \frac{y_{i+1}^2 + y_i^2}{4}\, \delta t_i - \frac{e^{-\frac{1}{2}(X_{i+1}+y_{i+1})^2} + e^{-\frac{1}{2}(X_i+y_i)^2}}{2}\, \delta t_i \Bigg] \end{aligned} \tag{65}$$

This expression is quite general and valid for any contour of integration in the complex time plane.

It is convenient to use $z_{i,j}$, $j = 1, \ldots, 4$, to denote the four variables Re X_i, Im X_i, Re y_i, Im y_i. The equations of motion are given by

$$\frac{\partial S}{\partial z_{i,j}} = 0 \qquad i = 1 \ldots N-1 \tag{66}$$

These amount to $4N-4$ conditions for the $4N+4$ unknowns $z_{i,j}$. The solution must also satisfy the boundary conditions

$$y_0 + y_1 - \frac{\imath}{\omega}(y_1 - y_0) = e^{\theta}\Big[y_0^* + y_1^* - \frac{\imath}{\omega}(y_1^* - y_0^*)\Big] \tag{67}$$

[cfr. Eq. (58), (60)] and

$$\text{Im } X_{N-1} = \text{Im } X_N = \text{Im } y_{N-1} = \text{Im } y_N = 0\ . \tag{68}$$

In addition, we remove the invariance under time translation by demanding that X_0 takes a fixed real value

$$X_0 = c \tag{69}$$

The precise value of c is not relevant. The only important criterion that c must satisfy is that the imaginary time axis falls between the expected

singular points of the solution. The value of c can be readjusted, if necessary, so that the point in the complex time plane where $\mathrm{Re}X = 0$ belongs to the CD part of the contour.

Equations (67)-(69) provide the required 8 additional conditions on the variables $z_{i,j}$. We will write these equations as

$$B_k(z_{i,j}) = 0 \tag{70}$$

Starting from the periodic instanton solutions and evolving them further from C to B we obtain an initial class of solutions to Eq. (66), (70) with $\theta = 0$. If we perform a small change of either θ or T, the two parameters which indirectly determine ν and ϵ, the field configuration $z_{i,j}$ will no longer satisfy the equations of motion. We seek a correction $\delta z_{i,j}$ such that $z_{i,j}+\delta z_{i,j}$ obey the equations of motion with new values for θ and/or T:

$$\left.\frac{\partial S}{\partial z_{i,j}}\right|_{z+\delta z} = 0 \tag{71}$$

$$B_k(z_{i,j} + \delta z_{i,j}) = 0 \tag{72}$$

If the deformation of the original solution is not too large, Eq. (71), (72) can be solved by the Newton-Raphson method: we expand to first order in δz and solve the linearized equations

$$\sum_{i',j'} \left.\frac{\partial^2 S}{\partial z_{i,j}\partial z_{i',j'}}\right|_z \delta z_{i',j'} = -\left.\frac{\partial S}{\partial z_{i,j}}\right|_z \tag{73}$$

$$\sum_{i',j'} \left.\frac{\partial B_k}{\partial z_{i',j'}}\right|_z \delta z_{i',j'} = -B_k\Big|_z \tag{74}$$

This procedure is repeated until it converges to a solution.

In our calculations we typically took $N = 2048$ and used the following computational strategy. Equation (73) with a definite index i only couples the variables $\delta z_{i',j}$ with $i' = i-1,\ i,\ i+1$. It is then possible to use an elimination procedure similar to the one outlined in Sect. 3 (see Eq. (40) and considerations that follow) and express all variables $\delta z_{i,j}$ in terms of $\delta z_{0,j}$, $\delta z_{N,j}$. (In practice this can be done maintaining complex variables notation, which simplifies the arithmetic. One must work with the explicit real and imaginary parts of the variables only at the next stage of the calculation.) Finally $\delta z_{0,j}$, $\delta z_{N,j}$, and $\delta z_{1,j}$, $\delta z_{N-1,j}$ which, by virtue of the elimination procedure are

now expressed as linear functions of $\delta z_{0,j}$, $\delta z_{N,j}$, are inserted into Eq. (74). These equations thus become a system of 8 real, linear, non-homogeneous equations in the 8 real variables $\delta z_{0,j}$, $\delta z_{N,j}$, that can be straightforwardly solved. We are then able to start from $\theta = 0$ (periodic instanton solution) and gradually increase θ to a very large value, which makes the incoming oscillator number ν effectively zero. At the same time we gradually reduce the value of T, which has the effect of increasing the energy ϵ. It is important to check that the solutions correspond indeed to tunneling processes, namely that in the further evolution along the positive real time axis the center of mass coordinate X goes to $+\infty$. We found this to be the case up to $\epsilon \sim 1.1$. At that point, though, the Newton-Raphson method develops an instability and, when convergence is eventually reached, further evolution along the real time axis shows a bounce from the barrier with $X \to -\infty$. We attribute this difficulty to the proximity of solutions with $X \to +\infty$ and $X \to -\infty$, with possible bifurcation points. In order to avoid falling into a solution without tunneling, we continue a tunneling solution to a positive real value of t along a contour extending into Im $t < 0$, as illustrated by the dashed line in Fig. 4. At the final value of t (point E in the graph of Fig. 4) the system is far into the positive X domain and we can further increase ϵ without running into any instability.

We illustrate in Fig. 7 a typical tunneling solution in the complex time plane. The figure displays the center of mass coordinate X as function of Re t, Im t (we inverted the direction of the Im t axis for a better perspective). The height of the surface gives the value of Re X, while the phase of the complex variable X is coded by color (red for real negative, blue for real positive, with the other values of the complex phase arranged in rainbow pattern—the color will appear as gray-scale in a black and white printout). The contour of integration of the equations of motion is indicated by a line of different color drawn on the surface. The continuation of X to the entire complex plane has been obtained by starting form the values along the imaginary time axis and integrating the equations of motion outward with the leapfrog algorithm. The singularities in the solution are quite apparent from Fig. 7. We found it noteworthy that one can determine the singularity structure of the solutions numerically, since ordinarily one would expect numerical integration methods to fail in the presence of a singularity. The integration algorithm becomes unstable and diverges as one approaches a singularity. However it is possible to exhibit the singularity structure by numerically integrating the solution along closed contours around the singularities. Integration of the equations

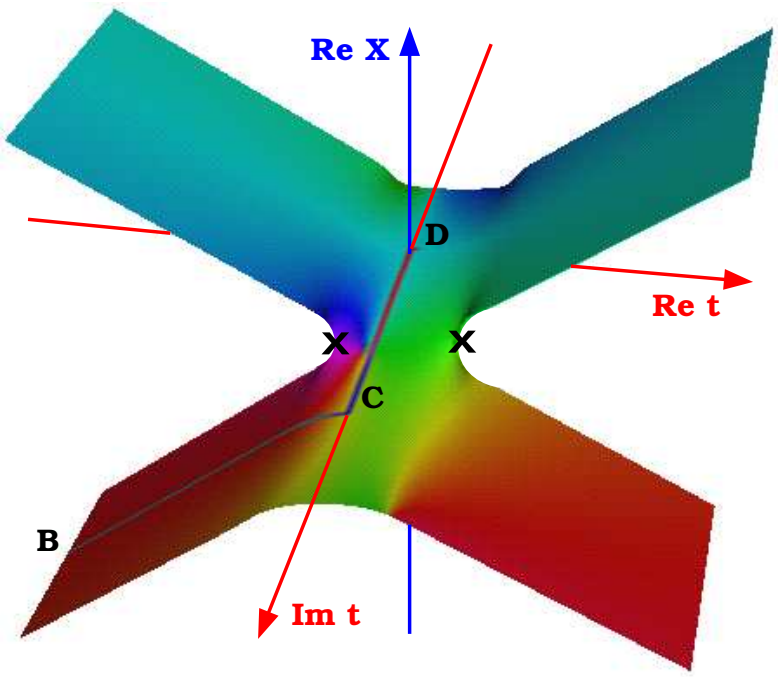

Figure 7: Tunneling solution to the equations of motion: center-of-mass coordinate as function of complex time. The singularities (branch points) are labeled by crosses.

of motion by the leapfrog algorithm along a closed contour entirely contained within a domain of analyticity produces final values for X and y identical to the initial values to high degree of numerical accuracy, equal to the expected discretization error $O((\delta t)^2)$ of the algorithm, whereas an enclosed singularity is clearly present when the initial and final values of X and y are different.

We reproduce in Table 3 the results of our semiclassical calculation. The data correspond to $\theta = 13$. In Figure 8 we present a comparison of the results for the exponent F_0 in the transmission probability (cfr. Eq.(1)) obtained with the full quantum-mechanical calculation (x) and with the semiclassical technique (solid line). In the quantum-mechanical calculation we extracted F_0 from the slope of the last segment in the graph of $\log \mathcal{T}_0$ versus $1/g^2$ at given energy for which we had meaningful data (see Fig. 3). As a consequence, the line defined by the crosses in Fig. 8 exhibits some small

$T/2$	ϵ	F	$T/2$	ϵ	F
1.75	1.0463	0.9715	0.35	1.4869	0.1038
1.72	1.0846	0.8386	0.3	1.5208	0.0817
1.7	1.1223	0.7103	0.25	1.5585	0.0611
1.6	1.1334	0.6734	0.2	1.6005	0.0422
1.4	1.1595	0.5950	0.175	1.6234	0.0336
1.2	1.1921	0.5103	0.15	1.6477	0.0257
1.0	1.2333	0.4195	0.125	1.6736	0.0186
0.8	1.2867	0.3235	0.1	1.7011	0.0124
0.7	1.3196	0.2741	0.075	1.7306	0.0073
0.6	1.3578	0.2244	0.05	1.7621	0.0034
0.5	1.4027	0.1749	0.0025	1.7960	0.0008
0.4	1.4560	0.1268	0.01	1.8176	0.0001

Table 3: Results of the semiclassical analysis.

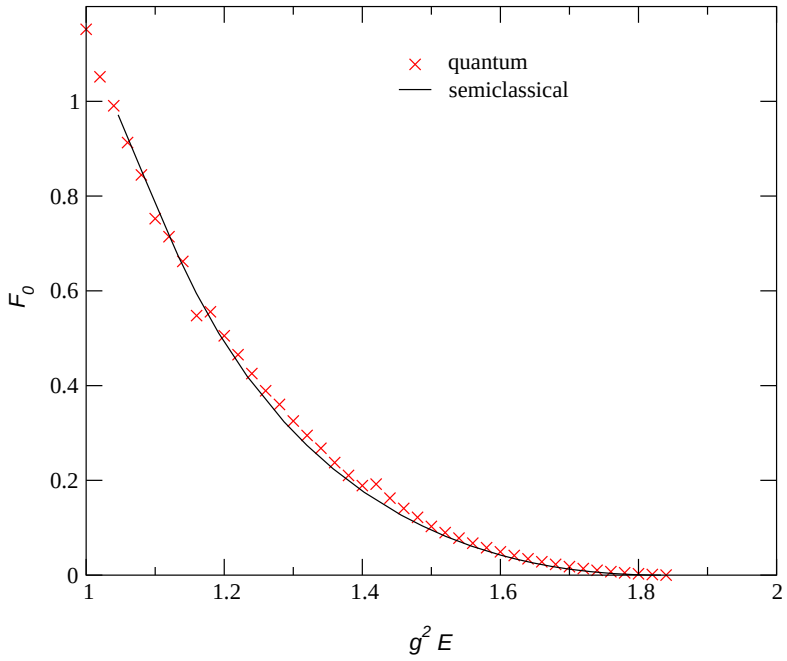

Figure 8: Comparison of the quantum mechanical and semiclassical results.

discontinuities. We take the magnitude of these discontinuities as an indication of the systematic errors in the quantum-mechanical calculation due to the neglect of perturbative $O(g^2)$ and higher order effects. Within these errors, the agreement between the results of the full quantum-mechanical calculation and of the semiclassical calculation is excellent.

5 Conclusions

Our results validate, in the context of a model calculation, the scaling formula of Eq. (1), (9), the applicability of the method of Ref. [1, 2] and the assumption that the ground state transition probability can be obtained as the limit of a more general transition probability from a coherent initial state.

At the same time our investigation has brought to light interesting properties of the analytic continuation of classical solutions to complex time and complex phase space. While the extension of classical motion to the complex time domain has long formed the mainstay of semiclassical calculations of tunneling, we believe that our specific application shows novel features of the analytically continued solutions intimately connected to the presence of several degrees of freedom. Of particular relevance we find that one can obtain information on the singularity structure of the solutions by numerical techniques.

With the qualification that a field has an infinite number of degrees of freedom while our model has only two, our results bode well for the application of the technique of Ref. [1, 2] to field theoretical processes. Hopefully, they will also open the path to new, imaginative applications of semiclassical methods in other challenging quantum-mechanical problems.

Ackowledgements. The authors are indebted to P. Tinyakov for helpful discussions. This research was supported in part under DOE grant DE-FG02-91ER40676, RFBR grant 96-02-17449a, and by the U.S. Civilian Research and Development Foundation for Independent States of FSU (CRDF) award RP1-187. Two of the authors (C.R. and V.R.) would like to thank Professor Miguel Virasoro for hopsitality at the Abdus Salam International Center for Theoretical Physics, where part of this work was carried out.

References

[1] V. A. Rubakov and P. G. Tinyakov. Towards the semiclassical calculability of high-energy instanton cross-sections. *Phys. Lett.*, B279:165–168, 1992.

[2] V. A. Rubakov, D. T. Son, and P. G. Tinyakov. Classical boundary value problem for instanton transitions at high-energies. *Phys. Lett.*, B287:342, 1992.

[3] A. N. Kuznetsov and P. G. Tinyakov. False vacuum decay induced by particle collisions. *Phys. Rev.*, D56:1156–1169, 1997.

[4] A. N. Kuznetsov and P. G. Tinyakov. Numerical study of induced false vacuum decay at high- energies. *Mod. Phys. Lett.*, A11:479–490, 1996.

[5] P. G. Tinyakov. Multiparticle instanton induced processes and b violation in high-energy collisions. *Phys. Lett.*, B284:410–416, 1992.

[6] A. H. Mueller. Comparing two particle and multiparticle initiated processes in the one instanton sector. *Nucl. Phys.*, B401:93–115, 1993.

[7] Michael P. Mattis. The riddle of high-energy baryon number violation. *Phys. Rept.*, 214:159–221, 1992.

[8] P. G. Tinyakov. Instanton like transitions in high-energy collisions. *Int. J. Mod. Phys.*, A8:1823–1886, 1993.

[9] V. A. Rubakov and M. E. Shaposhnikov. Electroweak baryon number nonconservation in the early universe and in high-energy collisions. *Usp. Fiz. Nauk*, 166:493–537, 1996.

[10] F. R. Klinkhamer and N. S. Manton. A saddle point solution in the weinberg-salam theory. *Phys. Rev.*, D30:2212, 1984.

[11] Claudio Rebbi and Jr. Robert Singleton. Computational study of baryon number violation in high- energy electroweak collisions. *Phys. Rev.*, D54:1020–1043, 1996.

[12] S. Yu. Khlebnikov, V. A. Rubakov, and P. G. Tinyakov. Periodic instantons and scattering amplitudes. *Nucl. Phys.*, B367:334, 1991.